



# Temperature distribution of cubic boron nitride–coated cutting tools by finite element analysis

Luqiang Tu<sup>1</sup> · Feng Xu<sup>1</sup> · Xue Wang<sup>1</sup> · Jiye Gao<sup>1</sup> · Shuai Tian<sup>1</sup> · Muk-Fung Yuen<sup>2</sup> · Dunwen Zuo<sup>1</sup>

Received: 6 June 2019 / Accepted: 20 September 2019 / Published online: 11 November 2019  
© Springer-Verlag London Ltd., part of Springer Nature 2019

## Abstract

Heat generation in cutting process has a great influence on performance and lifetime of cutting tools. Cubic boron nitride (cBN), combination of exceptional thermal conductivity and hardness, is a promising super-hard material as protective coatings on the cutting tools. However, the temperature distributions of micron-thickness coatings on cutting tools are very difficult to be examined by experiment methods. In this paper, finite element method (FEM) simulation was introduced to determine the temperature distribution of cBN/diamond coatings on silicon nitride ( $\text{Si}_3\text{N}_4$ ) cutting tools with various parameters compared with titanium aluminum nitride (TiAlN) coatings. The finite element (FE) model of cBN/diamond–coated  $\text{Si}_3\text{N}_4$  tools was built and validated by machining experiments. The effects of cutting speed and tool rake angle on temperature distribution of cBN/diamond–coated tools were investigated compared to TiAlN coatings based on developed model. The results show that the temperature is increased with the increase of cutting speed while decreased with the increase of tool rake angle. The temperature of cBN-coated tools is decreased by approximately 20.4–28.6% than TiAlN-coated tools under identical conditions. Additionally, the preferred cutting speed and rake angle were obtained among employed cutting parameters. The results demonstrated that using advanced cBN coatings can substantially improve the cutting performance of the tools. This work may offer a guideline to explore the temperature distribution of cBN-coated cutting tools in mechanical machining application for machining difficult-to-cut ferrous materials.

**Keywords** Cubic boron nitride coatings · Cutting tools · Finite element model · Temperature distribution

## 1 Introduction

Metal machining process involves the coupling effects of metal physical behaviors, including large strain, high strain rate, and extreme temperature. Plastic deformation of the

workpiece can dramatically produce heat at cutting regions in machining difficult-to-cut materials [1, 2]. Extreme temperature not only affects surface quality of workpiece but also contributes to the thermal deformation and failure of the cutting tools [3]. In order to guarantee the superior performance and longer service lifetime of cutting tools and to achieve lower costs and higher productivity in cutting process, the super-hard materials have been attracted so much attention in cutting tools applications [2].

Cubic boron nitride (cBN) is the second most thermally conductive and the second hardest material comparable to diamond. Additionally, cBN has high thermal stability and excellent chemical inertness against ferrous materials at temperatures up to 1200 °C, but diamond reacts with ferrous metal at 600 °C [2, 4]. The versatile combination of the remarkable physical and chemical properties of cBN renders it the most promising solution in machining difficult-to-cut ferrous components harder than 45 HRC such as hardened steel and hardened ductile iron [2, 5, 6]. Currently, the commercially available cBN cutting tools can only be fabricated by using

### Highlights

- Temperatures of the cubic boron nitride (cBN)/diamond coatings on silicon nitride ( $\text{Si}_3\text{N}_4$ ) cutting tools were analyzed systematically by finite element methods.
- Lower heat generation by using the cBN-coated cutting tools than commercial titanium aluminum nitride (TiAlN)–coated cutting tools was observed.
- Higher heat dissipation of cBN/diamond coatings than TiAlN coatings was obtained.

✉ Feng Xu  
xufeng@nuaa.edu.cn

<sup>1</sup> College of Mechanical and Electrical Engineering, Nanjing University of Aeronautics and Astronautics, Nanjing 210016, China

<sup>2</sup> School of Science and Engineering, The Chinese University of Hong Kong, Shenzhen 518172, Guangdong, China

**Table 1** Cutting parameters employed for cutting experiments

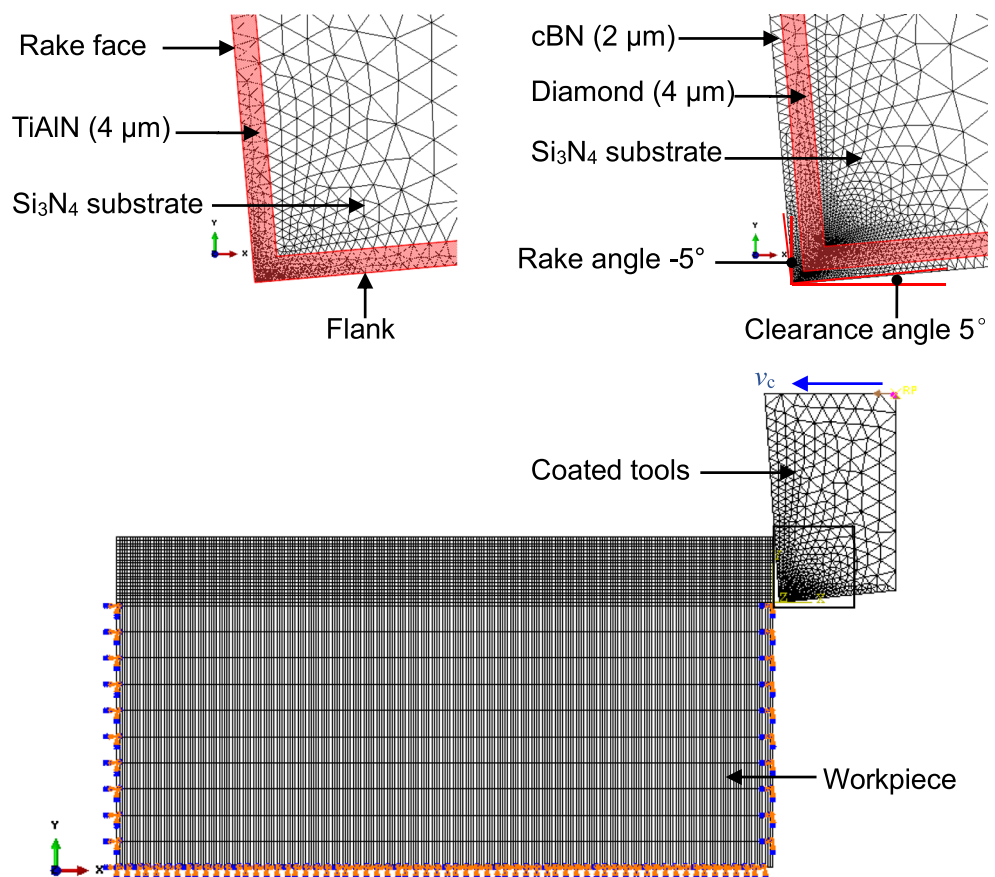
Test	Cutting speed, $v_c$ (m/min)	Feed rate, $f$ (mm/r)	Depth of cut, $a_p$ (mm)
1	63	0.10	0.05; 0.10; 0.15; 0.20; 0.25
2	60; 80; 120; 190	0.15	0.25
3	96; 119; 191; 239	0.20	0.25

cBN powders synthesized by high-pressure high-temperature (HPHT) method, which is costly and difficult to achieve complex geometries. The cBN-coated cutting tools by employing coatings technique (e.g., PVD and CVD) have higher flexibility and lower cost than polycrystalline cBN (PcBN) tools fabricated by HPHT [4].

Up to now, cBN coatings, however, have not been used in industrial cutting tools because of the difficulty in the deposition process including limitations of coating thickness and insufficient mechanical stability, which resulted from considerable compressive stress and poor adhesion between coatings and substrates [4]. Only a few works on laboratory level, mainly devoted to the research on deposition and cutting performance of cBN-coated cutting tools, have been addressed. Among these works, most of them focused on deposition of

cBN-coated cutting tools but still lacked the evaluation of performance by implementing cutting experiments [7–10]. Although several works investigated the cutting performance of cBN-coated cutting tools, they merely focused on the cutting force and tool wear [11–13]. Unfortunately, the research on cutting temperature of cBN-coated cutting tools remains an unexploited territory. The limited success of these attempts in the evaluation of performance for cBN-coated tools motivated us to explore the temperature distributions, and we expected to complement this drawback.

In our previous work, the 2.2- $\mu\text{m}$ -thick cBN coatings have been successfully deposited on  $\text{Si}_3\text{N}_4$  cutting tools via boron-doped diamond (BDD) buffer layers by the electron cyclotron resonance microwave plasma chemical vapor deposition (ECR MPCVD) technique [14]. And the mechanical and

**Fig. 1** Configuration of tool-workpiece for the FEM simulation

**Table 2** Physical properties of the workpiece [21, 32]

Density (kg/m <sup>3</sup> )	Young's modulus (GPa)	Poisson's ratio	Thermal conductivity (W/m °C)
7320	176	0.275	30

friction wear performances of cBN-coated Si<sub>3</sub>N<sub>4</sub> cutting tools have been evaluated by comparison with TiAlN coatings [14]. Since cBN, diamond, and Si<sub>3</sub>N<sub>4</sub> are all electrical insulator [15], the infrared thermography methods were introduced to measure the cutting temperature in our turning experiments. This method can measure temperature without physical contact, and also, it is of fast response and high capability of providing the thermal fields [16, 17]. However, the temperature distributions of micron-thickness coatings on cutting tools are very difficult to be captured by infrared thermography methods owing to the micro-scale coatings and the rapid response of heat transfer. The finite element method (FEM) has been an alternative and helpfully complementary technique to better understand the temperature field distribution for machining process [18, 19].

In this paper, a series of experimental and numerically simulated studies were carried out to investigate the influence of cutting parameters on the temperature distribution of cBN/diamond-coated Si<sub>3</sub>N<sub>4</sub> cutting tools. FE model of cBN/diamond-coated tools was built and validated by turning experiments. In addition, FEM simulations of the temperature distribution of cBN/diamond coatings on Si<sub>3</sub>N<sub>4</sub> cutting tools with various cutting speed and tool rake angle were implemented. This study may provide a guideline for further exploring the temperature distribution in experimental machining difficult-to-cut ferrous materials by applying cBN-coated cutting tools.

## 2 Experimental and modelling

### 2.1 Experimental procedure

The cylindrical workpiece used in the cutting experiments was made from hardened ductile iron (QT900) with a hardness of ~54 HRC obtained by heat treatment process. Ductile iron has outstanding properties including extreme strength, high toughness, and excellent wear resistance. Thus, it has been

**Table 3** Thermal expansion of the workpiece [21, 32]

Temperature (°C)	20–100	200	300	400	500	600	700
Thermal expansion (×10 <sup>-6</sup> /°C)	11.5	11.8	12.6	13.2	13.4	13.5	13.8

extensively employed as an important engineering material for the fabrication of tribological components such as crankshafts, wind turbine elements, gear, railway brake discs, and motor frames [20–23]. The as-deposited cBN/diamond-coated Si<sub>3</sub>N<sub>4</sub> cutting tools were employed. Additionally, the commercial TiAlN-coated Si<sub>3</sub>N<sub>4</sub> cutting tools were selected as references which have excellent thermal stability and cutting performance in machining ferrous metals, as reported by [24–27]. Cutting experiments were carried out on a CA6140 lathe employing cylindrical turning under dry conditions. During the experiments, the cutting tools were mounted on tool holders (CRSNR2525M12, ZCCCT, Co., Ltd., China), and combination of the cutting tools and holders resulted in an effective negative rake angle of 5° and an effective clearance angle of 5°. A triaxial piezoelectric force sensor (Kistler 9265B) with a data acquisition system was used to continuously monitor cutting forces components. The temperatures during cutting process were measured by an infrared thermometer (Thermovision A20). The cutting parameters employed in the cutting experiments are displayed in Table 1.

### 2.2 Finite element modelling

The two-dimensional thermo-viscoplastic cutting simulation model was conducted for the two coated cutting tools by using a commercial Abaqus/Explicit software. The proposed finite element model is illustrated in Fig. 1. In the finite element model, each coating layer is represented by separate layer of respective thickness, cBN (2 μm)/diamond (4 μm) and TiAlN (4 μm) on top of the Si<sub>3</sub>N<sub>4</sub> substrate, see Fig. 1. The bottom surface of the workpiece is fixed in all directions. The cutting tool is assumed as a rigid body and is moved forward with the cutting speed (*v<sub>c</sub>*). The cutting simulation is performed at ambient temperature assuming the initial temperature is equal to 25 °C.

The Coulomb friction model is the most widely used in the simulation of metal cutting process [28, 29]. To express the friction contact between tool rake face, flank, and workpiece, the extended Coulomb friction model is adopted in this study. The relationship between shear stress and friction coefficient of the tool-chip contact is described by the following [30, 31]:

$$\tau = \begin{cases} \mu\sigma_n, & \mu\sigma_n < \tau_{\max} \\ \tau_{\max}, & \mu\sigma_n \geq \tau_{\max} \end{cases} \quad (1)$$

where  $\tau$  is shear stress,  $\mu$  is friction coefficient,  $\sigma_n$  is the normal contact pressure,  $\tau_{\max}$  is the shear limit stress,  $\tau_{\max} = \frac{\sigma_{Mises}}{\sqrt{3}}$ , and  $\sigma_{Mises}$  is the Mises yield stress. In this study, the friction coefficient of cBN coatings and TiAlN coatings with the workpiece was set to be 0.17 and 0.3, respectively.

The physical parameters of workpiece and coated cutting tools are displayed in Tables 2, 3, 4, and 5.

Providing the physical and thermal parameters of the workpiece, cutting tools, and coating materials is of great

**Table 4** Specific heat capacity of the workpiece [21, 32]

Temperature (°C)	20–200	300	400	500	600	700	800	1200	1350
Specific heat (J/kg °C)	461	494	507	515	536	603	750	917	963

importance to obtain reliable results from the finite element solution. Most importantly, these materials undertake the behavior of high strain, strain rate and extreme temperature in cutting process [29]. The Johnson-Cook material model is suitable for describing high rate deformation of materials and can produce excellent results for chip formation [39, 40]. The workpiece material was modeled as isotropic thermal-elastic plastic body expressed by

$$\sigma = (A + B\varepsilon^n) \left[ 1 + C \ln \left( \frac{\dot{\varepsilon}}{\dot{\varepsilon}_0} \right) \right] \left[ 1 - \left( \frac{T - T_r}{T_m - T_r} \right)^m \right] \quad (2)$$

where  $A$ ,  $B$ ,  $n$ ,  $C$ , and  $m$  are material parameters, i.e.,  $A$  is the yield stress,  $B$  is the strain hardening factor,  $n$  is the strain hardening index,  $C$  is the strain rate sensitivity parameter,  $m$  is the thermal softening index;  $\sigma$  is equivalent stress,  $\varepsilon^n$  is equivalent plastic strain, and  $\dot{\varepsilon}$  and  $\dot{\varepsilon}_0$  are equivalent plastic strain rate and reference strain rate, respectively; and  $T$  is the homologous temperature and  $T_r$  and  $T_m$  are reference ambient temperature and material melting temperature, respectively. The Johnson-Cook parameters for workpiece materials are listed in Table 6.

The Johnson-Cook damage initiation law is employed to define material failure process in the FE model [41], as given by

$$\bar{\varepsilon}_D^{pl} = \left[ d_1 + d_2 \exp \left( d_3 \frac{\sigma_p}{\sigma_{Mises}} \right) \right] \left[ 1 + d_4 \ln \frac{\xi}{\xi_0} \right] \left[ 1 + d_5 \left( \frac{T - T_r}{T_m - T_r} \right)^m \right] \quad (3)$$

where  $\sigma_p$  is the hydro static pressure,  $\sigma_{Mises}$  is Mises stress,  $\xi_0$  is reference strain rate, generally equals to 1,  $\xi$  is equivalent plastic strain rate,  $\bar{\varepsilon}_D^{pl}$  is equivalent plastic strain of damage initiation, and  $d_1$ – $d_5$  are failure parameters and the values for

workpiece are displayed in Table 7. The cutting parameters employed for simulation are listed in Table 8.

### 3 Validation of the finite element model

The cutting force and cutting temperature of finite element results are compared with cutting experiments results to verify the effectiveness and correctness of finite element model proposed.

#### 3.1 Cutting force

Figure 2 depicts the radial force simulated and experimental dependent on depth of cut ( $a_p$ ) for TiAlN- and cBN-coated cutting tools at  $v_c$  of 63 m/min. It can be found that the cutting force increases with the increase of  $a_p$  for each cutting tool. And cBN-coated tools show lower cutting force than TiAlN-coated tools. It could be attributed to the lower friction coefficient and higher hardness of cBN coatings than TiAlN coatings, which have been demonstrated in our previous study [14]. For cutting tools, low friction coefficient can decrease the friction forces between tools and workpieces and evacuate effectively the chips from the tool rake face; high hardness can enhance the wear resistance against tool wear and maintain the superior cutting performance reported by Davim [2]. The relative errors of simulated and experimental results are lower than 18% of both cBN- and TiAlN-coated tools. The errors could be attributed to the applied friction law in finite element modelling [28, 42].

Figure 3 shows that the radial force decreases with the increase of cutting speed ( $v_c$ ) for TiAlN- and cBN-coated cutting tools at  $a_p$  of 0.25 mm. This could be ascribed to the effect of increasing in temperature. Uzun et al. [28] and Ng et al. [37] have demonstrated that with the increase of  $v_c$ , cutting temperature at the first deformation zone increases but the yield strength of the workpiece decreases, leading to the decrease of cutting force. Additionally, cBN-coated tool shows the lower cutting force than TiAlN-coated tools. It is attributed to the lower friction coefficient and excellent wear

**Table 5** Physical properties of the cutting tools [14, 15, 33–38]

	Friction coefficient	Thermal conductivity (W/m °C)	Thermal expansion ( $\times 10^{-6}/^\circ\text{C}$ )	Specific heat (J/kg °C)	Density (kg/m <sup>3</sup> )	Young’s modulus (GPa)	Poisson’s ratio
TiAlN	0.3	50	7.5	500	1892	350	0.171
cBN	0.17	1300	0.59	1000	3490	850	0.128
Diamond	– <sup>a</sup>	2000	0.8	800	3515	1000	0.115
Si <sub>3</sub> N <sub>4</sub>	– <sup>a</sup>	100	2.11	600	3210	210	0.201

<sup>a</sup> The dispensable parameters in this study



**Table 6** Johnson-Cook parameters of workpiece [39, 40]

<i>A</i> (MPa)	<i>B</i> (MPa)	<i>n</i>	<i>C</i>	<i>m</i>	<i>T<sub>m</sub></i> (°C)	<i>T<sub>r</sub></i> (°C)	Hardness (HRC)
1150	739	0.26	0.014	1.03	1460	25	54

resistance of cBN coatings. And the relative errors of simulated and experimental results are low than 12% for both cBN- and TiAlN-coated cutting tools.

### 3.2 Cutting temperature

Figure 4 shows the simulated and experimental cutting temperature as a function of cutting speed ( $v_c$ ) for TiAlN- and cBN-coated cutting tools at  $a_p$  of 0.25 mm. Figure 5 illustrates the simulated and experimental cutting temperature, and Fig. 5b is the infrared images obtained from turning procedure by using cBN-coated cutting tools at  $v_c$  of 239 m/min. The inset is the image of turning operation. The cutting temperature increases with the increase of  $v_c$  (as shown in Fig. 4). This can be ascribed to the workpiece plastic deformation and chip sliding. With the increase of  $v_c$ , the workpiece plastic deformation rate and the chip sliding velocity are increased, which induce a more rapid heat formation, thus resulting in the increase of cutting temperature demonstrated by Uzun et al. [28], Ng et al. [37], and Khalili et al. [43].

Moreover, the cutting temperature obtained by using cBN-coated tool is lower than that by TiAlN-coated tools (as depicted in Fig. 4). The main reasons are the lower friction coefficient and higher thermal conductivity of cBN coatings. The research results of Ng et al. [37], Kone et al. [44], and Grzesik [45] have demonstrated that the properties of coatings on cutting tools have significant influence on heat generation and dissipation, although the heat dissipation by tools is less than that by the chips. Lower friction coefficient induces less friction; higher thermal conductivity yields more rapid heat dissipation under identical conditions. Additionally, the relative errors of simulated and experimental results are low than 14% for both cBN- and TiAlN-coated tools.

The relative errors of simulated and experimental results for cutting force and cutting temperature are acceptable and reasonable in some extent. The temperature at tool-chip contact region, where the maximum temperature is produced, cannot be measured by infrared method in cutting experiments. Thus,

**Table 7** Failure parameters of workpiece [41]

$d_1$	$d_2$	$d_3$	$d_4$	$d_5$
-0.8	2.1	-0.5	0.0002	0.61

the experimental cutting temperature is lower than that of simulated results. Together with the above results verified that the proposed FM model is effective and correct. Therefore, the finite element model can be employed to predict coated tools temperature distribution and evolution at various cutting parameters.

## 4 Simulated results and discussion

### 4.1 Comparison of cutting temperature distribution by using TiAlN- and cBN-coated tools

Among the cutting parameters, involving cutting speed ( $v_c$ ), feed rate ( $f$ ), and depth of cut ( $a_p$ ), the  $v_c$  has the most significant effect on the cutting temperature reported by Davim [2]. Thus, the influence of  $v_c$  on cutting temperature is studied mainly in this paper.

The distributions of cutting temperature by using cBN- and TiAlN-coated tools at  $v_c$  of 150 m/min are shown in Fig. 6. The temperatures for both cutting tools and chips show the obvious gradient distribution. The maximum temperature occurs at the chips particularly the contact region between tools and chips, since the heat generation sources are mostly from the intensive friction of tool-chip interfaces and the large plastic deformation of chip under extreme conditions is demonstrated by Uzun et al. [28]. Additionally, the cutting temperature obtained by applying cBN-coated tools is lower than that by TiAlN-coated tools, indicating the less heat generation during turning by cBN-coated tools. It is noted that the temperature distribution of tool flank face-workpiece is not shown in Fig. 6. Under the cutting conditions of negative rake angle  $5^\circ$  and positive clearance angle  $5^\circ$ , the rake face and chips experienced the more intensive friction and deformation which is the mainly source of cutting heat, as demonstrated by Fig. 5b.

### 4.2 Effect of cutting speed on TiAlN- and cBN-coated tools temperature

Generally, the temperature in the cutting tools is lower than the temperature resided in chips. This can be ascribed to following two aspects. Firstly, the chips experience not only the

**Table 8** Cutting parameters employed for simulation

Test	Cutting speed, $v_c$ (m/min)	Depth of cut, $a_p$ (mm)
1	63	0.05; 0.10; 0.15; 0.20; 0.25
2	60; 80; 120; 190	0.25
3	96; 119; 191; 239	0.25
4	150	0.30
5	210; 250; 290; 330	0.50
6	270	0.40

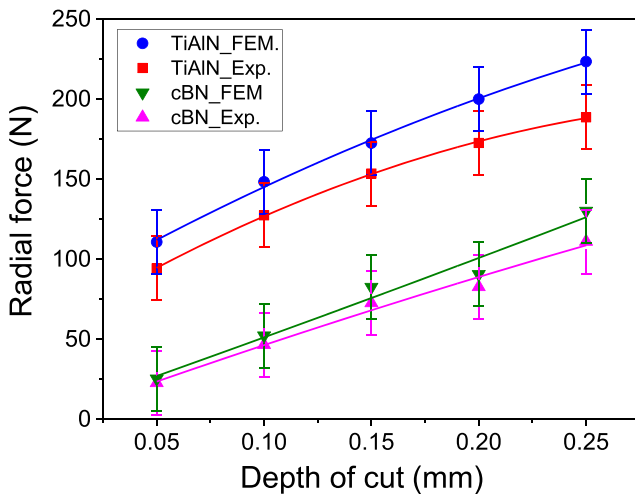


**Fig. 2** Radial force simulated and experimental dependent on depth of cut for TiAlN- and cBN-coated cutting tools at  $v_c$  of 63 m/min

intensive friction but also the plastic deformation generated by the extrusion of cutting tools. But the cutting tools only undergoes the friction resulted from the chips and workpiece due to its higher hardness than workpiece. Additionally, the thermal contact conductance of tool-chip interface affects heat transfer; thus, the cutting heat transferred to the cutting tools is reduced [28, 46, 47]. More importantly, the heat transferred to the tools can greatly affect the cutting performance of the tools demonstrated by Grzesik [48, 49]. Therefore, it is indispensable to investigate the temperature distribution in the coated tools. Figure 7 shows the maximum temperature of TiAlN- and cBN-coated cutting tools obtained by FEM simulation as a function of cutting speed at  $a_p$  of 0.50 mm. It is revealed that the temperature is increased with the increase of cutting speed for both TiAlN- and cBN-coated cutting tools.

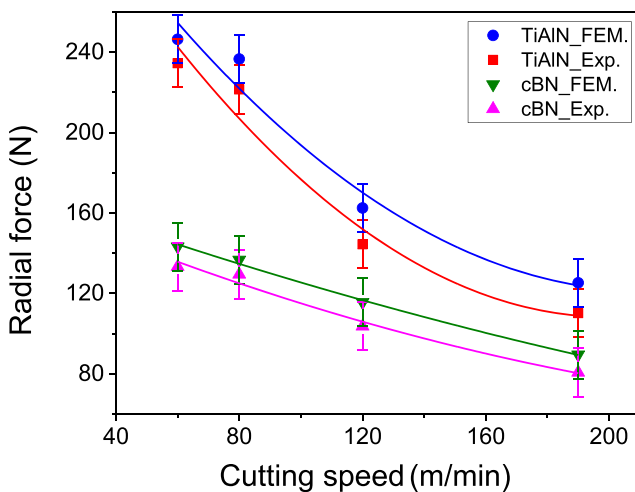


**Fig. 3** Radial force simulated and experimental dependent on cutting speed for TiAlN- and cBN-coated cutting tools at  $a_p$  of 0.25 mm

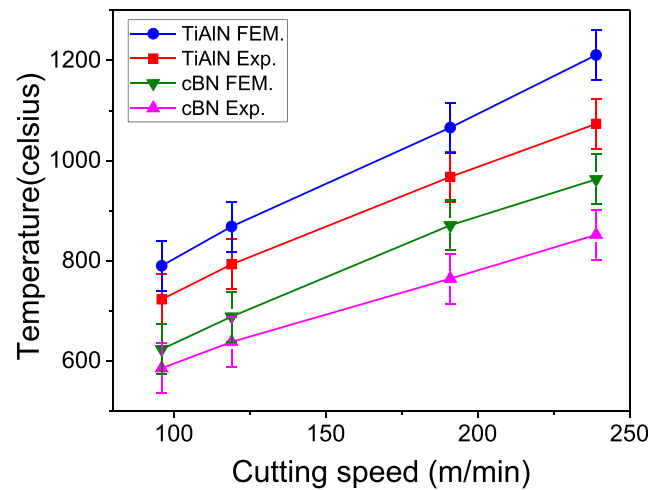


**Fig. 4** Cutting temperature simulated and experimental dependent on cutting speed for TiAlN- and cBN-coated cutting tools at  $a_p$  of 0.25 mm

In order to better understand the heat distribution and dissipation of each coating with substrates, we mainly studied the temperature variation of coatings regions under enlarged view conditions. Figure 8 depicts the temperature distribution of TiAlN- and cBN/diamond-coated  $\text{Si}_3\text{N}_4$  cutting tools. It is shown that maximum temperature of cBN/diamond-coated tools is significantly lower than TiAlN-coated tools, which indicates the less heat generation of cBN coatings. Cubic BN coatings have lower coefficient than that of TiAlN coatings, which has been demonstrated by implementing friction and wear experiments in our previous study [14], thus contributing to less heat generation during cutting process. Moreover, each coating and tool substrate shows relatively obvious gradient distribution of temperature. The heat dissipation in cBN/diamond coating regions is more rapid than TiAlN coatings under the same conditions. The disparity is mainly attributed to the thermal conductivity of coating and substrate material. For coating materials, higher thermal conductivity enables a rapid heat dissipation illustrated by Grzesik [45]. Furthermore, maximum temperature is resided in the rake face and decreased with the increase of depth in cutting tools. Coatings for both TiAlN and cBN/diamond, as the heat-isolation layers, maintain the tool substrate a relatively low temperature. This is ascribed to the disparity from thermal conductivity of materials and thermal contact conductance of coating-tool substrate interfaces reported by Courbon et al. [47] and Grzesik [48].

In combination of the above simulated results, it is found that the maximum temperature occurs at tool rake face. The rake face not only undergoes extreme temperature but also experiences intensive friction from chips, thus leading to severe tool wear. In addition, the thermal stability of TiAlN coatings and cBN coatings are 800 °C and 1200 °C, respectively [4, 14, 50]. Considering the temperature, rake face

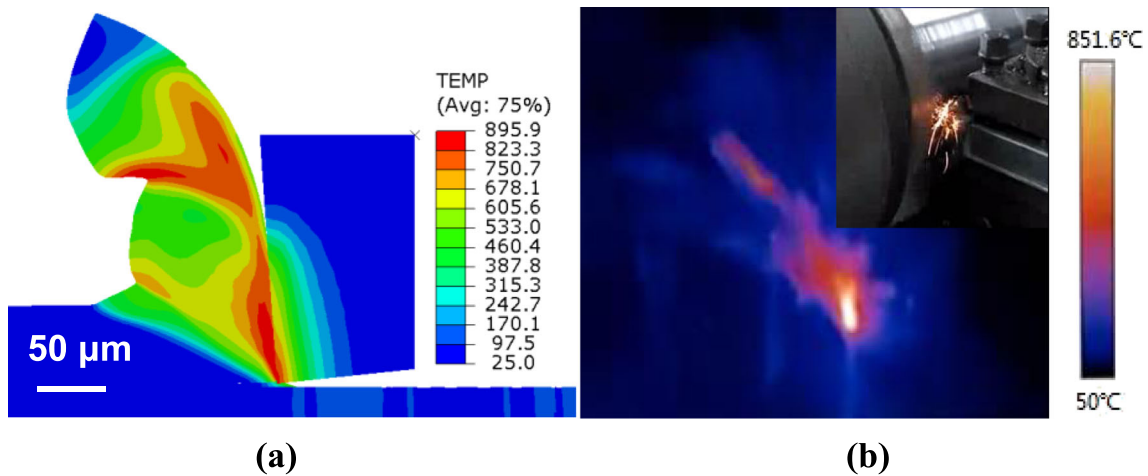


**Fig. 5** Cutting temperature of **a** simulated results and **b** experimental results obtained infrared image from turning procedure by using cBN-coated cutting tools at  $v_c$  of 239 m/min. The inset is turning operation

wear, and thermal stability of coatings, we concluded that the preferred cutting speed among employed cutting parameters is below 250 m/min for TiAlN-coated cutting tools while cBN-coated cutting tools has a wide range of cutting speed to be adopted.

### 4.3 Effect of rake angle on TiAlN- and cBN-coated tools temperature

Tool geometry has a significant influence on the cutting temperature, cutting force, and tool life during turning process. Generally, the negative rake angle ( $\gamma_0$ ) and positive clearance angle ( $\alpha_0$ ) are recommended for machining difficult-to-cut materials (above 47 HRC) such as hardened steels, tool steels, and hardened ductile iron reported by Davim [2].

Figure 9 shows the maximum temperature in TiAlN- and cBN-coated tools as a function of the rake angle with the constant  $v_c$  of 270 m/min and constant clearance angle of 5°.

It is noted that the temperature decreases with the increase of rake angle, indicating the proper increase of tool rake angle can reduce the tool temperature. Hu et al. [51] have demonstrated that relatively large rake angle not only can improve friction state of tool surface but also can reduce chip deformation during turning process, thus leading to less heat generation. Additionally, the temperature of cBN-coated cutting tools is decreased by approximately 20.4–28.6% than that of TiAlN-coated cutting tools. This is ascribed to the lower friction coefficient of cBN coatings than TiAlN coatings demonstrated in our previous study [14].

Figure 10 shows the temperature distributions of TiAlN- and cBN/diamond-coated cutting tools with different rake angles at constant clearance angle (5°) and constant cutting speed (270 m/min). The temperatures show the obvious gradient distribution for TiAlN and cBN/diamond coatings with tool substrates. And the maximum temperature occurs at rake face, then it propagates and decreases with the increase of depth in cutting

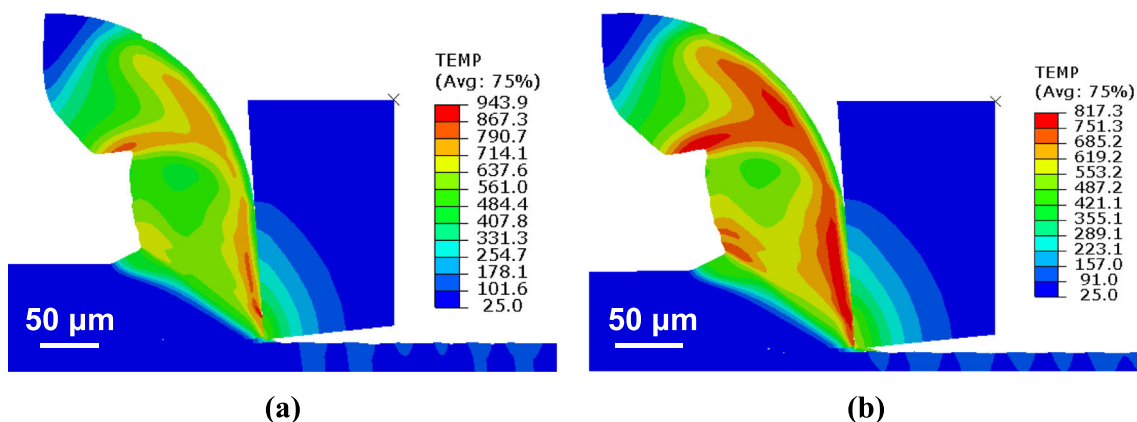


**Fig. 6** Cutting temperature simulated by using **a** TiAlN- and **b** cBN-coated cutting tools at  $v_c$  of 150 m/min

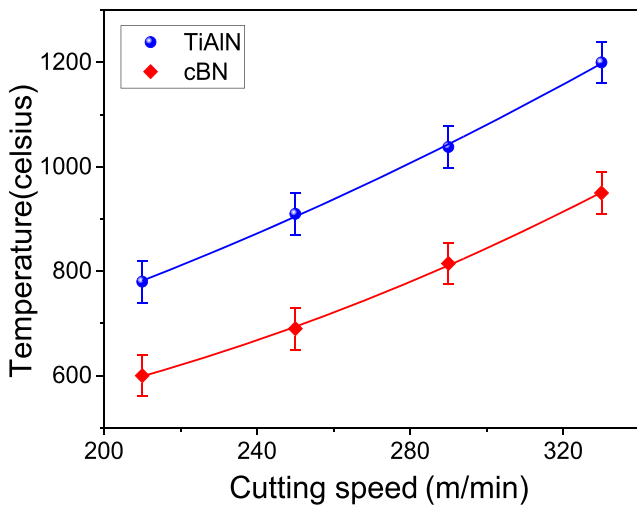


Fig. 7 Tool maximum temperature obtained simulation dependent on cutting speed for TiAlN- and cBN-coated cutting tools at  $a_p$  of 0.50 mm

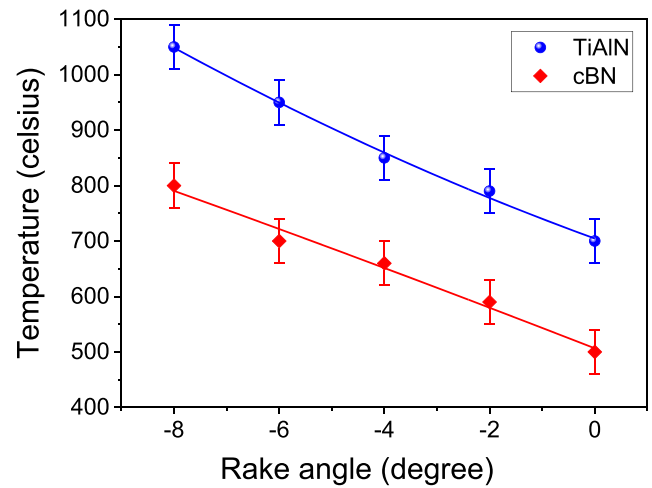


Fig. 9 Tool maximum temperature obtained simulation dependent on rake angle for TiAlN- and cBN/diamond-coated  $Si_3N_4$  cutting tools with the constant clearance angle of  $5^\circ$  and the constant  $v_c$  of 270 m/min

tools. Furthermore, the dissipation of cBN/diamond coatings is more rapid than TiAlN coatings under identical conditions. It should be attributed to the higher thermal conductivity of cBN

and diamond, rendering the rapid heat dissipation. When the rake angle was increased to be  $-2^\circ$ , the temperature is decreased for both TiAlN- and cBN/diamond-coated cutting

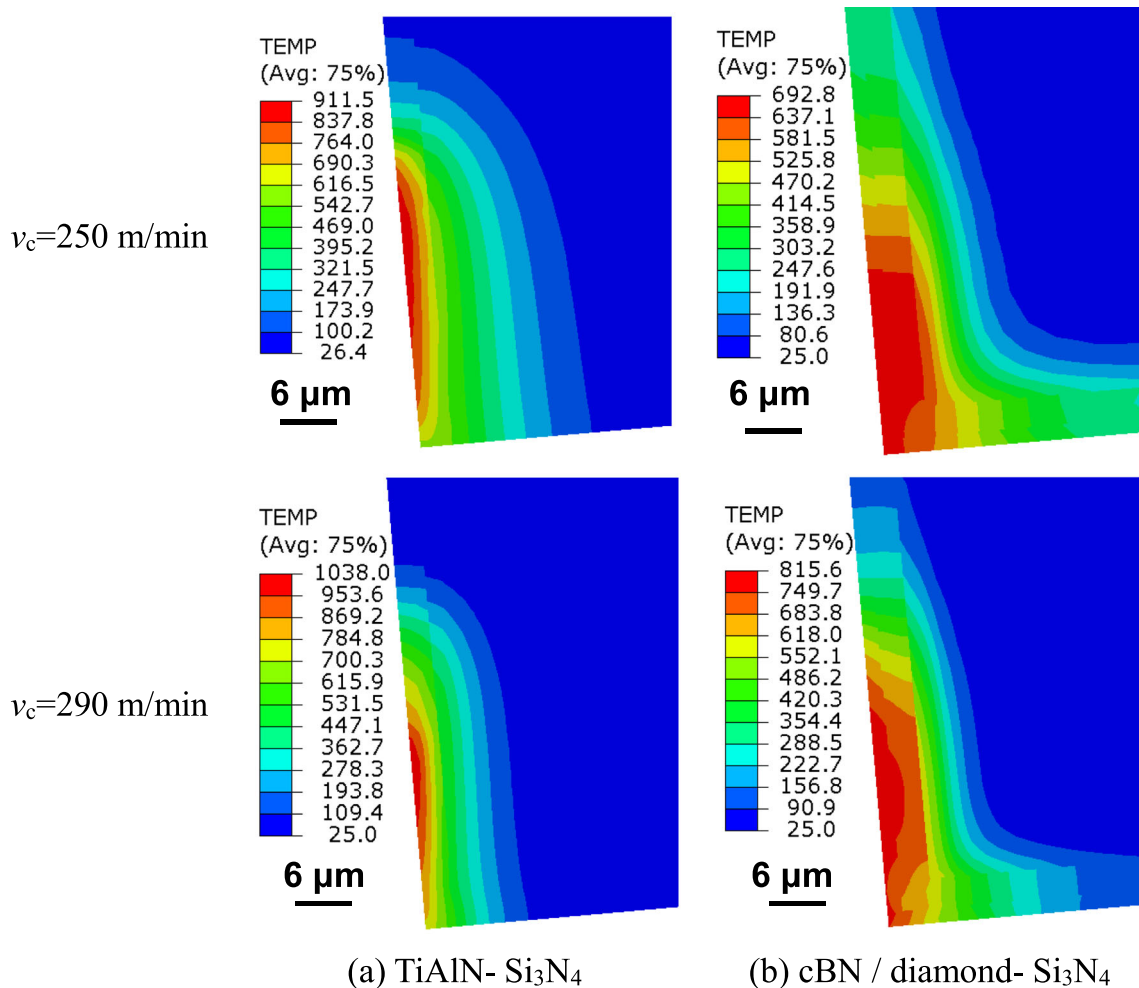
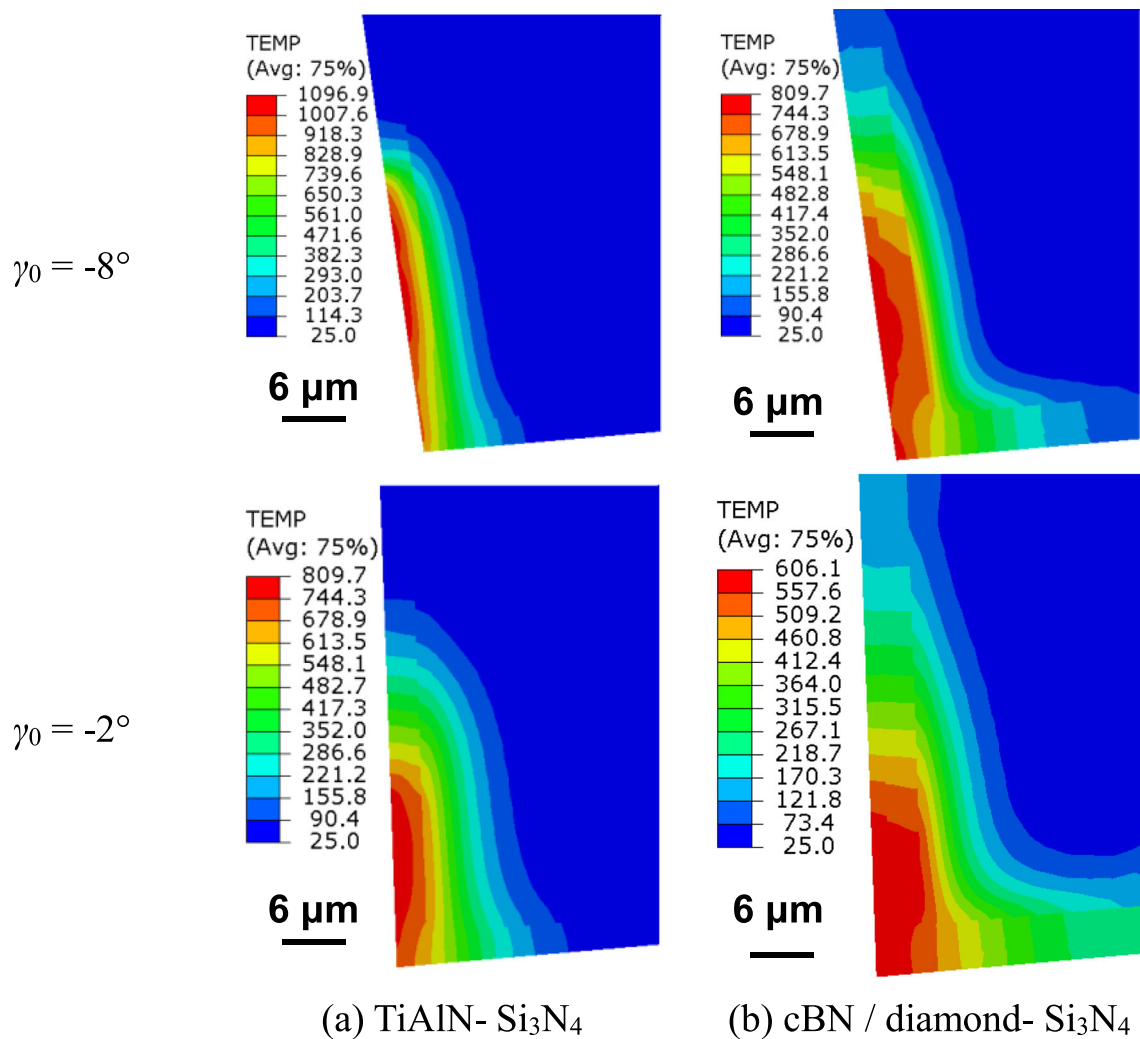


Fig. 8 Temperature distribution simulated of a TiAlN- and b cBN/diamond-coated  $Si_3N_4$  cutting tools at  $v_c$  of 250 and 290 m/min





**Fig. 10** Tool temperature distribution simulated of **a** TiAlN- and **b** cBN/diamond-coated  $\text{Si}_3\text{N}_4$  cutting tools at rake angle of  $-8^\circ$  and  $-2^\circ$  and the constant clearance angle of  $5^\circ$  and constant  $v_c$  of 270 m/min

tools. And the maximum temperature still resides in rake face, but its rich region transfers to near the tool nose. The decreasing of temperature could be ascribed to the larger rake angle improves friction status of between tool rake face and chips and reduces intensive chip deformation [51].

Considering the temperature, rake face wear, and thermal stability of coatings, we concluded that the preferred tool rake angle among selected cutting parameters is above  $-4^\circ$  for TiAlN-coated cutting tools. But the cBN-coated cutting tools have a wide range of tool rake angle to be used.

## 5 Conclusion

Finite element method simulation was introduced to determine the temperature distribution of cBN/diamond-coated  $\text{Si}_3\text{N}_4$  cutting tools. The FE model of cBN/diamond-coated

tools was built and validated by turning experiments. Based on the developed FE model, the effects of cutting speed and tool rake angle on temperature distribution of cBN/diamond-coated tools were investigated compared to TiAlN coatings. The results show that the temperature is increased with the increase of cutting speed while decreased with the increase of tool rake angle. The maximum temperature occurred at the rake face and then decreased dramatically with the increase of tool depth. The temperature of cBN-coated tools is decreased by approximately 20.4–28.6% than TiAlN-coated tools under identical conditions. Additionally, the preferred cutting speed and rake angle were obtained among employed cutting parameters in consideration of the temperature, rake face wear, and thermal stability of coatings. The results showed that the use of advanced cBN coatings can significantly improve the performance of cutting tools with distinctly lower temperature than the commercial TiAlN coatings.

**Funding information** This work was supported by the National Natural Science Foundation of China (Nos. 51575269, 51562027) and the Six Talent Peaks Project in Jiangsu Province of China (No. ZBZZ-005).

## References

- Kryzhanivskyy V, Bushlya V, Gutnichenko O, M'Saoubi R, Stahl J-E (2018) Heat flux in metal cutting: Experiment, model, and comparative analysis. *Int J Mach Tools Manuf* 134:81–97
- Davim JP (2011) *Machining of hard materials*. Springer, London
- Zhang WQ, Wang XL, Hu YJ, Wang SY (2018) Predictive modeling of microstructure changes, micro-hardness and residual stress in machining of 304 austenitic stainless steel. *Int J Mach Tools Manuf* 130–131:36–48
- Zhang WJ, Chong YM, He B, Bello I, Lee ST (2014) Cubic boron nitride films: properties and applications. In: *Comprehensive hard materials*. Elsevier, Boston, pp 607–639
- Devries RC (1972) *Cubic boron nitride: handbook of properties*. General Electric Company, Boston
- Bonfa MM, Costa ES, Sales WF, Amorim FL, Maia LHA, Machado AR (2019) Evaluation of tool life and workpiece surface roughness in turning of AISI D6 hardened steel using PCBN tools and minimum quantity of lubricant (MQL) applied at different directions. *Int J Adv Manuf Technol* 103(1–4):971–984
- Teii K, Hori T, Matsumoto S (2011) Enhanced deposition of cubic boron nitride films on roughened silicon and tungsten carbide-cobalt surfaces. *Thin Solid Films* 519(6):1817–1820
- Teii K, Matsumoto S (2012) Direct deposition of cubic boron nitride films on tungsten carbide-cobalt. *ACS Appl Mater Interfaces* 4(10):5249–5255
- Stein C, Keunecke M, Bewilogua K, Chudoba T, Kolker W, Berg H (2011) Cubic boron nitride based coating systems with different interlayers for cutting inserts. *Surf Coat Technol* 205(4):103–106
- Chong YM, Zhang WJ, Yang Y, Ye Q, Bello I, Lee ST (2009) Deposition of cubic boron nitride films on diamond-coated WC: Co inserts. *Diam Relat Mater* 18(11):1387–1392
- Keunecke M, Wiemann E, Weigel K, Park ST, Bewilogua K (2006) Thick c-BN coatings- preparation, properties and application tests. *Thin Solid Films* 515(3):967–972
- Uhlmann E, Fuentes JAO, Keunecke M (2009) Machining of high performance workpiece materials with CBN coated cutting tools. *Thin Solid Films* 518(5):1451–1454
- Jiang W, Malshe AP (2011) A novel cBN composite coating design and machine testing: a case study in turning. *Surf Coat Technol* 206(2–3):273–279
- Xu F, Yuen MF, He B, Wang CD, Zhao XR, Tang XL, Zuo DW, Zhang WJ (2014) Microstructure and tribological properties of cubic boron nitride films on  $\text{Si}_3\text{N}_4$  inserts via boron-doped diamond buffer layers. *Diam Relat Mater* 49:9–13
- Liu HM (1995) *Diamond chemical vapor deposition: nucleation and early growth stages*. Noyes Publications, Park Ridge
- Saez-de-Buruaga M, Soler D, Aristimuno PX, Esnaola JA, Arrazola PJ (2018) Determining tool/chip temperatures from thermography measurements in metal cutting. *Appl Therm Eng* 145:305–314
- Artzoul J, Lescahier C, Bomont O, Dudzinski D (2014) Extended infrared thermography applied to orthogonal cutting: mechanical and thermal aspects. *Appl Therm Eng* 64:441–452
- Sadeghifar M, Sedaghati R, Jomaa W, Songmene V (2018) A comprehensive review of finite element modeling of orthogonal machining process: chip formation and surface integrity predictions. *Int J Adv Manuf Technol* 96:3747–3791
- Shetty N, Shahabaz SM, Sharma SS, Shetty SD (2017) A review on finite element method for machining of composite materials. *Compos Struct* 176:790–802
- Harding RA, Gilbert GNJ (1986) Why the properties of ductile irons should interest engineers. *Br Foundrym* 79:489–496
- Dodd J (1987) High strength, high ductility ductile irons. *Mod Cast* 68(5):60–66
- Zeng DF, Lu LT, Zhang YB, Zhang JW (2017) Investigation on the scuffing resistance of ductile cast iron as affected by fine particle bombardment to produce surface hardened layer and micro-dimpled surface. *Wear* 378–379:174–182
- Foglio E, Lusuardi D, Pola A, La-Vecchia GM, Gelfi M (2016) Fatigue design of heavy section ductile irons: influence of chunky graphite. *Mater Des* 111:353–361
- Uhlmann E, Riemer H, Schroter D, Henze S, Sammler F, Barthelma F, Frank H (2018) Investigation of wear resistance of coated PcBN turning tools for hard machining. *Int J Refract Met Hard Mater* 72: 270–275
- Galoppi GD, Filho MS, Batalha GF (2006) Hard turning of tempered DIN 100Cr6 steel with coated and no-coated CBN inserts. *J Mater Process Technol* 179(1–3):146–153
- Grzesik W, Rech J, Zak K, Claudin C (2009) Machining performance of pearlitic-ferritic nodular cast iron with coated carbide and silicon nitride ceramic tools. *Int J Mach Tools Manuf* 49(2):125–133
- Grzesik W, Malecka J (2011) Documentation of tool wear progress in the machining of nodular ductile iron with silicon nitride-based ceramic tools. *CIRP Ann Manuf Technol* 60(1):121–124
- Ucun I, Aslantas K (2011) Numerical simulation of orthogonal machining process using multilayer and single-layer coated tools. *Int J Adv Manuf Technol* 54(9–12):899–910
- Ozel T (2006) The influence of friction models on finite element simulations of machining. *Int J Mach Tools Manuf* 46(5):518–530
- Chen G, Ren CZ, Zhang P, Cui KH, Li YC (2013) Measurement and finite element simulation of micro-cutting temperatures of tool tip and workpiece. *Int J Mach Tools Manuf* 75(12):16–26
- Zhu Z, To S, Zhu WL, Huang P, Zhou X (2019) Cutting forces in fast-/slow tool servo diamond turning of micro-structured surfaces. *Int J Mach Tools Manuf* 136:62–75
- Labrecque C, Gagne M (1998) Ductile iron: fifty years of continuous development. *Can Metall Q* 37(5):343–378
- Bello I, Chong YM, Leung KM, Chan CY, Ma KL, Zhang WJ, Lee ST, Layous A (2005) Cubic boron nitride films for industrial applications. *Diam Relat Mater* 14(11–12):1784–1790
- Huang Y, Liang SY (2003) Cutting forces modeling considering the effect of tool thermal property-application to CBN hard turning. *Int J Mach Tools Manuf* 43(3):307–315
- Rachbauer R, Gengler JJ, Voevodin AA, Resch K, Mayrhofer PH (2012) Temperature driven evolution of thermal, electrical, and optical properties of Ti-Al-N coatings. *Acta Mater* 60(5):2091–2096
- Shatla M, Kerk C, Altan T (2001) Process modeling in machining. Part II: validation and applications of the determined flow stress data. *Int J Mach Tools Manuf* 41(11):1659–1680
- Ng EG, Aspinwall DK, Brazil D, Monaghan J (1999) Modeling of temperature and forces when orthogonally machining hardened steel. *Int J Mach Tools Manuf* 39(6):885–903
- Bartosik M, Holec D, Apel D, Klaus M, Genzel C, Keckes J, Arndt M, Polcik P, Koller CM, Mayrhofer PH (2017) Thermal expansion of Ti-Al-N and Cr-Al-N coatings. *Scripta Mater* 127:182–185
- Johnson GR, Cook WH (1983) A constitutive model and data for metals subjected to large strains, high strain rates and high temperature. *Proceedings of the Seventh International Symposium on Ballistics, Netherlands*, pp 541–547
- Coelho RT, Ng EG, Elbestawi MA (2007) Tool wear when turning hardened AISI 4340 with coated PcBN tools using finishing cutting conditions. *Int J Mach Tools Manuf* 47(2):263–272
- Johnson GR, Cook WH (1985) Fracture characteristics of three metals subjected to various strains, strain rates, temperatures and pressures. *Eng Fract Mech* 21:31–48

42. Arrazola PJ, Aristimuno P, Soler D, Childs T (2015) Metal cutting experiments and modelling for improved determination of chip/tool contact temperature by infrared thermography. *CIRP Ann Manuf Technol* 64(1):57–60
43. Khalili K, Safaei M (2009) FEM analysis edge preparation for chamfered tools. *Int J Mater Form* 2:217–224
44. Kone F, Czarnota C, Haddag B, Nouari M (2011) Finite element modelling of the thermo-mechanical behavior of coatings under extreme contact loading in dry machining. *Surf Coat Technol* 205(12):3559–3566
45. Grzesik W (1999) Experimental investigation of the cutting temperature when turning with coated indexable inserts. *Int J Mach Tools Manuf* 39(3):355–369
46. Norouzifard V, Hamed M (2014) Experimental determination of the tool-chip thermal contact conductance in machining process. *Int J Mach Tools Manuf* 84:45–57
47. Courbon C, Mabrouki T, Rech J, Mazuyer D, D'Eramo E (2013) On the existence of a thermal contact resistance at the tool-chip interface in dry cutting of AISI 1045: formation mechanisms and influence on the cutting process. *Appl Therm Eng* 50(1):1311–1325
48. Grzesik W (1998) The role of coatings in controlling the cutting process when turning with coated indexable inserts. *J Mater Process Technol* 79:133–143
49. Grzesik W (2000) An integrated approach to evaluating the tribo-contact for coated cutting inserts. *Wear* 240:9–18
50. Joshi A, Hu HS (1995) Oxidation behavior of titanium-aluminium nitrides. *Surf Coat Technol* 76-77:499–507
51. Hu HJ, Huang WJ (2014) Tool life models of nano ceramic tool for turning hard steel based on FEM simulation and experiments. *Ceram Int* 40(7):8987–8996

**Publisher's note** Springer Nature remains neutral with regard to jurisdictional claims in published maps and institutional affiliations.